Critical competition between two distinct orbital-spin ordered states in perovskite vanadates

J. Fujioka,[1,2] T. Yasue,[2] S. Miyasaka,[2,3] Y. Yamasaki,[2] T. Arima,[4,5] H. Sagayama,[4] T. Inami,[6] K. Ishii,[6] and Y. Tokura[1,2,7]

[1]*Multiferroics Project, ERATO, Japan Science and Technology Agency, Wako 351-0198, Japan*

[2]*Department of Applied Physics, University of Tokyo, Tokyo 113-8656, Japan*

[3]*Department of Physics, Graduate School of Science, Osaka University, Osaka 560-0043, Japan*

[4]*Institute of Multidisciplinary Research for Advanced Materials, Tohoku University, Sendai 980-8577, Japan*

[5]*RIKEN SPring-8 Center, Hyogo 679-5148, Japan*

[6]*Synchrotron Radiation Research Unit, Japan Atomic Energy Agency, Hyogo 679-5148, Japan*

[7]*Cross-Correlated Materials Research Group (CMRG) and Correlated Electron Research Group (CERG), RIKEN Advanced Science Institute, Wako 351-0198, Japan*

(Received 7 June 2010; revised manuscript received 27 September 2010; published 18 October 2010)

We have investigated the spin/orbital phase diagram in the perovskite orthovanadate $R\mathrm{VO}_3$ (R=Eu, Y, Dy, and Ho) by measurements of magnetization, dielectric constant, specific heat, Raman scattering spectra, and x-ray diffraction, focusing on the interplay between the V $3d$ spin and the $4f$ moment of the R ion. The thermally induced phase transition between the C-type spin/G-type orbital ordered state and the G-type spin/C-type orbital ordered state is observed for $\mathrm{Eu}_{1-x}\mathrm{Y}_x\mathrm{VO}_3$ (x=0–0.52) without $4f$ moment. By comparing this phase diagram with the spin/orbital ordering in TbVO_3, it is evident that the critical competition between the C-type spin/G-type orbital ordered phase and the G-type spin/C-type orbital ordered one depends not only on the GdFeO_3-type lattice distortion but also on the presence of the $4f$ moment of the R ion. The magnetic field induced phase transition of the spin/orbital ordering is achieved concomitantly with polarizing R $4f$ moments for DyVO_3 and HoVO_3. For DyVO_3, the G-type spin/C-type orbital ordered phase is switched to the C-type spin/G-type orbital ordered one by applying a moderate magnetic field around 3 T. By contrast, the G-type spin/C-type orbital ordering is rather favored under the magnetic field in HoVO_3. The results cannot be uniquely explained in terms of the exchange interaction between the V $3d$ spin and the R-ion $4f$ moment. The coupling of the R $4f$ moment polarization with the lattice distortion tied with the orbital ordering of the V $3d$ sublattice may also be relevant to this field induced phase transition.

DOI: 10.1103/PhysRevB.82.144425 PACS number(s): 75.25.Dk, 75.30.Kz, 71.30.+h

I. INTRODUCTION

Transition-metal oxides with perovskite and related structure have provided a variety of interesting phenomena arising from the strong electron correlation, such as Mott transition, high-T_c superconductivity, colossal magnetoresistance effect and so on.[1] In particular, the recent investigations on the colossal magnetoresistive manganese oxides have invoked a broad interest in the close interplay among spin, charge, and orbital degrees of freedom, and hence the orbital ordering (OO) and related phenomena have become the important topics in condensed matter physics.[2] In the manganites with the orbital-active e_g electrons, the charge/orbital ordered state competes with the ferromagnetic one, and results in the bicritical feature in the vicinity of the boundary between these phases. The charge/orbital ordering is melted by the various external stimuli, such as magnetic, electric fields, light/x-ray and electron irradiations, and consequently the phase transition from the charge/orbital ordered insulator to ferromagnetic metal occurs. The perovskite-type vanadium oxide, $R\mathrm{VO}_3$ (R=rare-earth elements and Y), with the orbital-active t_{2g} electrons is another prototype of the correlated electron system with orbital degrees of freedom, and shows the spin-orbital-lattice coupled phenomena.[3–8] This t_{2g} electron system exhibits two distinct orbital ordered states depending on the ionic radius of $R(r_R)$ and/or temperature, and the phase switching between these two long-range orbital ordered states is possible also by external stimuli. Such a phase transition from one orbital ordered state to another is rather rare while the phase transition observed in the colossal magnetoresistive manganites is viewed as the melting of the orbital ordering. Recently, such a switching of the orbital ordering by the external magnetic field has been reported in one of the perovskite-type vanadium oxides, DyVO_3.[8,9]

Perovskite-type vanadium oxides $R\mathrm{VO}_3$ have a $Pbnm$ ($P2_1/b2_1/n2_1/m$) orthorhombic structure with lattice constants of $a \sim b \sim c/\sqrt{2}$ at room temperature.[10–13] The two distinct patterns of the spin and orbital ordering in this system are schematically shown in Figs. 1(a) (C-type spin/G-type orbital ordering) and (b) (G-type spin/C-type orbital ordering). Figure 1(c) reproduces a spin/orbital phase diagram of $R\mathrm{VO}_3$. Some new data for $\mathrm{Pr}_{1-x}\mathrm{La}_x\mathrm{VO}_3$ are added here to improve/update the phase diagram (see Appendix).[3] As temperature is lowered, all $R\mathrm{VO}_3$ undergo a structural phase transition from $Pbnm$ orthorhombic to $P2_1/b$($P2_1/b11$) monoclinic crystal structure accompanied with the G-type OO, and also a magnetic transition from paramagnetic to the C-type spin ordering (SO).[11–14] In $R\mathrm{VO}_3$, two electrons are present in the t_{2g} sector of V^{3+} ions. Since the orthorhombic distortion causes a splitting of the energy level of the V^{3+} t_{2g} orbital, one electron always occupies the d_{xy} orbital and the other either the d_{yz} or the d_{zx} orbital. The occupied d_{yz} and d_{zx} orbitals are staggered in all three (x,y,z) directions (orbital G type) while the V^{3+} spins (S=1) are arranged ferromagnetically along the c axis and antiferromagnetically in the ab plane (spin C type). As shown in Fig. 1(c), the C-type

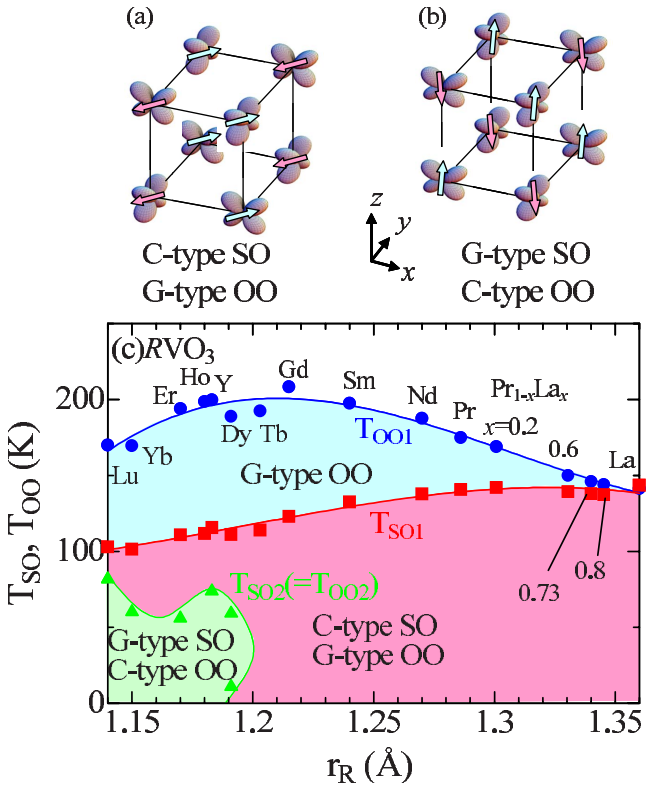

FIG. 1. (Color online) (a) Schematic view of the C-type spin ordering (SO) with the G-type orbital ordering (OO) (b) that of the G-type SO with the C-type OO. (c) Phase diagram of the spin/orbital ordering in RVO_3 (R is rare-earth ion). r_R is the ionic radii of R. See also Fig. 3 for the phase diagram in $Y_{1-x}Eu_xVO_3$. The filled circle, square, and triangle are T_{OO1}, T_{SO1}, and T_{SO2} ($=T_{OO2}$), respectively. The phase diagram is reproduced mainly from the result by Miyasaka *et al.* (Ref. 3) and also from some new data obtained in this study (see Appendix). The data T_{SO2} ($=T_{OO2}$) for R=Ho is omitted for clarity, which is discussed in Sec III C.

antiferromagnetic transition temperature (T_{SO1}) and the G-type orbital ordering one (T_{OO1}) depend on r_R. As r_R is increased from Lu to La, the $GdFeO_3$-type orthorhombic lattice distortion with the tilting of VO_6 octahedra and the cooperative Jahn-Teller distortion coupled with the G-type OO is gradually decreased. The decreasing V-O-V bond angle distortion increases the transfer integral and consequently enhances the magnetic and orbital exchange interactions between the nearest-neighbor V sites. T_{SO1} monotonically increases perhaps due to the increase in the exchange interaction, as the R ion is changed from Lu to La. On the other hand, T_{OO1} takes a maximum value around R=Gd and decreases toward R=La, as r_R increases. The nonmonotonous dependence of T_{OO1} on r_R is perhaps a result of the competition between the increase in the orbital exchange interaction and the suppression of the Jahn-Teller distortion. The investigation on the solid-solution series $Pr_{1-x}La_xVO_3$ clarifies the rather continuous change in T_{SO1} and T_{OO1} between R=Pr and La as discussed in Appendix.

In RVO_3 with small size R ions (R=Dy-Lu, and Y), another spin and orbital ordering pattern is known to show up as the ground state; that is, the G-type SO with the antiferromagnetic coupling between V^{3+} (S=1) spins in all the orthogonal directions and the C-type OO with the alternate $d^1_{xy}d^1_{yz}/d^1_{xy}d^1_{zx}$ electron configuration in the ab plane and the identical one along the c axis. One such compound is YVO_3, which shows a temperature-induced magnetization reversal phenomenon.[15] This compound undergoes the subsequent magnetic transition from the C-type to the G-type with decreasing temperature. Below this magnetic transition temperature ($T_{SO2}=T_{OO2}$), the pattern of the OO concomitantly turns into the C-type, accompanying the lattice structural change from the intermediate-temperature $P2_1/b$ to the lower-temperature $Pbnm$ symmetry coupled with the collective Jahn-Teller distortion.

As shown in Fig. 1(c), $DyVO_3$ is located in the close vicinity of the phase boundary between the two distinct spin/orbital ordered states in the phase diagram, and these ordered states compete with each other. In a previous paper,[9] we have investigated $DyVO_3$ by measurements of magnetization, Raman-scattering spectra, and x-ray diffraction. As temperature is lowered, the pattern of the spin/orbital ordering in this material shows the reentrant change, C→G→C type/G→C→G type, respectively. The phase transition at lower temperature is triggered by the ordering of the Dy 4f Ising moments. In the intermediate-temperature phase (G-type spin/C-type orbital ordering), the external magnetic field along the a and b axes ($H\|a$ and $H\|b$) induces the metamagnetic transition of the Dy 4f moments. The magnetic field alignment of the Dy 4f moment causes the rearrangement of the V 3d spins from G-type to C-type and accordingly the switching of the pattern of the occupied d_{yz}/d_{zx} orbitals from C type to G type. The temperature-induced reentrant transition and the magnetic field induced one between the C-type spin/G-type orbital ordered and the G-type spin/C-type orbital ordered states are related to the close interplay between the Dy 4f moments and the V 3d spin/orbital degree of freedom.

To clarify the mechanism of the strong correlation between the R 4f moment and the V 3d spin/orbital degrees of freedom, we have systematically investigated the spin/orbital ordering for RVO_3 (R=Eu, Y, Dy, and Ho) with changing the temperature, orthorhombic lattice distortion, and magnetic field. First, we have studied the spin/orbital ordering in single crystalline $Y_{1-x}Eu_xVO_3$ ($0\leq x\leq 1$), focusing on the competition between the bare 3d-electron spin/orbital ordered states on the V^{3+} ions. The choice of this mixed crystal of $EuVO_3$ and YVO_3, which are located near the phase boundary between the two distinct spin/orbital ordered states, enables us to systematically investigate the spin/orbital phase diagram with changing the lattice distortion governing the stability of the magnetic and orbital ordered states while eradicating the influence of the R 4f moment on the V 3d spins because of no magnetic moment for Eu^{3+} ($4f^6$) and Y^{3+} ($4f^0$) at low temperatures. In addition, we have comparatively studied the spin/orbital ordered states in $DyVO_3$ and $HoVO_3$ to further pursue the influence of the R 4f moments on the spin/orbital ordering of the V 3d electrons by measurements of magnetization, dielectric constant, and x-ray diffraction in the magnetic field.

II. EXPERIMENTAL METHODS

Polycrystalline powder of RVO_3 (R=$Y_{1-x}Eu_x$, Dy, Ho, and $Pr_{1-x}La_x$) was first prepared by solid-state reaction using

Eu_2O_3, Y_2O_3, Dy_2O_3, Ho_2O_3, La_2O_3, Pr_6O_{11}, and V_2O_5 as the starting materials. The mixed powders of the starting materials were reacted at 600 and 1200 °C in flow of forming gas of Ar/H_2 (93/7%). The ceramics were pulverized again and sintered at 1350 °C in the same condition. Then the powders were pressed into a rod (typically 5 mm $\times$100 mm) and sintered at 1500 °C for 10 h in flow of forming gas of Ar/H_2. The single crystal growth was performed on this sintered rod using a halogen-lamp image furnace at a rate of 20–30 mm/h under an atmosphere of pure Ar. The obtained crystals were pulverized and checked by powder x-ray diffraction with Cu $K\alpha$ radiation. The cation ratio of the grown crystals was also checked by the inductively coupled plasma atomic emission spectroscopy. The grown crystals of RVO_3 were confirmed to be detwinned between the *ac* and *bc* planes by Laue reflection and single-crystal x-ray diffraction with a four-circle diffractometer. The single crystals were oriented with use of the back-reflection Laue method, and cut into plates with the wide surfaces perpendicular to the crystallographic principal axes.

A measurement of magnetization was performed by using a superconducting quantum interference device magnetometer. The temperature and magnetic field dependence of dielectric constant was measured with an *LCR* meter (Agilent E4980) at a frequency of 10 kHz. Vacuum-deposited silver films onto the end faces of single crystalline RVO_3 were used as electrodes. In the measurements of polarized Raman spectra, light (0.5 mW) from an Ar ion laser (514.5 nm) was focused onto a spot in 0.01 mm diameter on the surface of *ab* plane, which was polished to optical flatness with alumina powder. For the present study, we employed the back-scattering configuration. The scattered light was dispersed by a triple monochromator and detected with a liquid-nitrogen-cooled charge-coupled device detector. The polarization of incident and scattered lights are parallel to the $(a \pm b)$ axis. This polarized geometry is described using the conventional notation of $z(xx)\bar{z}$, where optical axes, x, y, and z are taken parallel to the orthorhombic crystal axes, $a+b$, $a-b$, and c. The x-ray (401) Bragg reflection is allowed in the $P2_1/b$ monoclinic phase coupled with the G-type OO but is forbidden in the *Pbnm* orthorhombic one. The synchrotron-radiation x-ray diffraction was performed to detect this Bragg reflection and determine the orbital ordered patterns. Nonresonant single-crystal x-ray diffraction was measured at Beamlines 4C and 16A1, Photon Factory (PF) of KEK, and at Beamline 22XU, SPring-8. x-ray was monochromatized to 12 keV for Beamline 4C and 16A1, and to 18 keV for 22XU with Si (111) double crystals and focused on the sample in a cryostat equipped with a superconducting magnet. The Bragg reflections were measured in magnetic fields applied parallel to the a axis ($H \| a$) up to 6 T on the Beamline 22XU, and to the b-axis ($H \| b$) up to 5 T on 16A1. The specific heat was measured by a thermal relaxation method.

III. RESULTS AND DISCUSSION

A. Two-phase Competition in $Y_{1-x}Eu_xVO_3$

In this section, we discuss the spin/orbital ordering for $Y_{1-x}Eu_xVO_3$, in which the influence of the R $4f$ moment is negligible. Since r_A of Eu is larger than that of Y, the $GdFeO_3$-type orthorhombic lattice distortion is systematically reduced with increasing the Eu concentration (x). In Fig. 2(a), we show the temperature dependence of the magnetization for $H \| a$ in YVO_3 ($x=0$). As temperature is lowered, the magnetization shows successive anomalies; a kink and increase at 200 K ($=T_{OO1}$) and at 116 K ($=T_{SO1}$) corresponding to the onset of the G-type OO and C-type SO, respectively. With further lowering temperature, the magnetization shows a sign reversal around 95 K and a jump around 75 K (T_{SO2}) corresponding to the onset of the G-type SO coupled with the C-type OO. These are all in accord with the features reported in literature.[3,11,12,15,16] The thermal hysteresis of the magnetization curve indicates the first-order phase transition. Figures 2(b)–2(f) show the temperature dependence of the magnetization for various x. For $x=0-0.52$, the onset of the G-type spin/C-type orbital ordering at T_{SO2} ($=T_{OO2}$) manifests itself as a clear jump of the magnetization. On the other hand, for $x=0.6$ and 1.0, the jump in the magnetization curve is no longer discernible, indicating

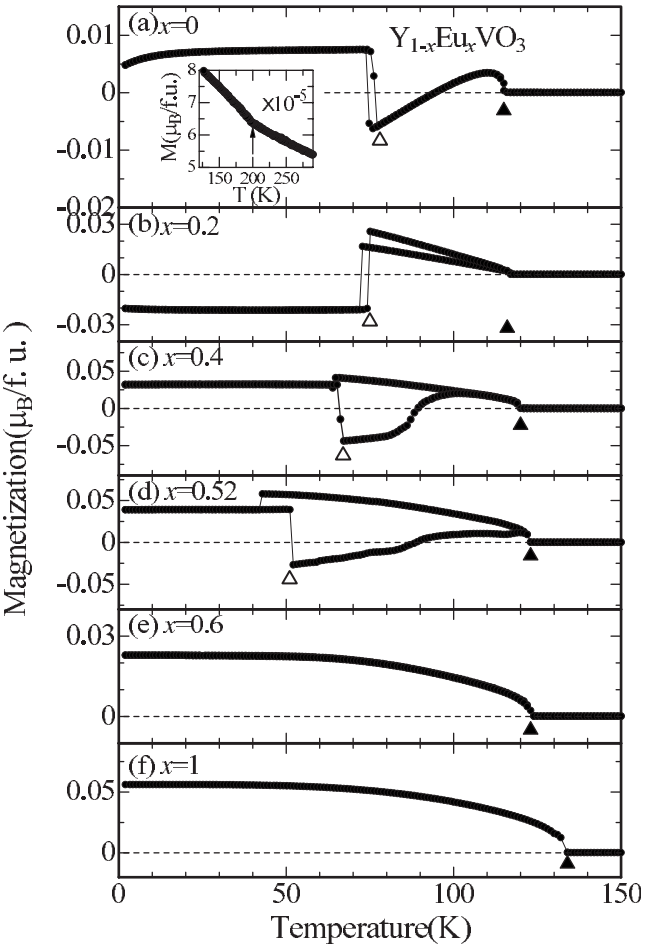

FIG. 2. Temperature dependence of the magnetization for $Y_{1-x}Eu_xVO_3$ with $x=0$, 0.2, 0.4, 0.52, 0.6, and 1.0 from (a) to (f), respectively. f.u. means formula units. Closed and open triangle denote T_{SO1} and T_{SO2} ($=T_{OO2}$) determined in the warming process, respectively. The inset of (a) is a magnified view of the magnetization curve in the temperature range from 120 to 290 K. Arrow indicates the onset of the G-type OO at T_{OO1}.

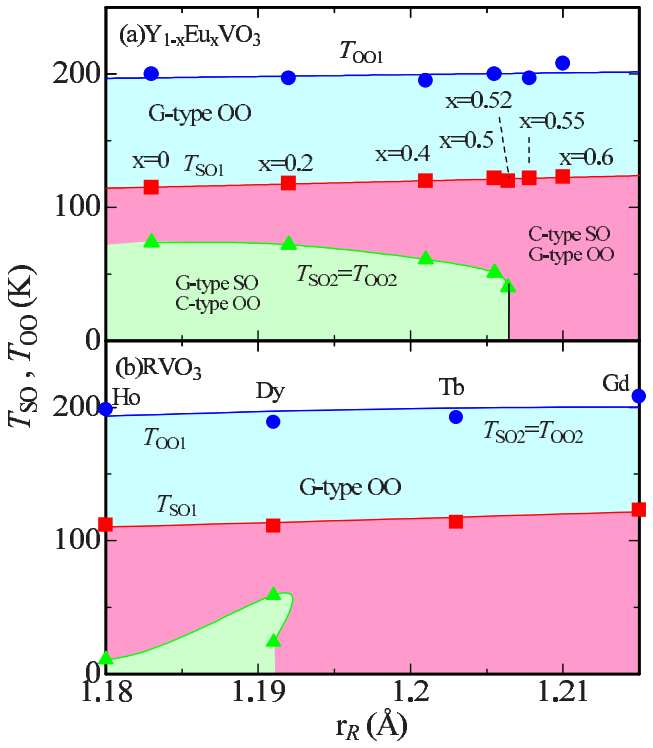

FIG. 3. (Color online) Phase diagram of the spin/orbital ordering for (a) $Y_{1-x}Eu_xVO_3$ and (b) RVO_3 (R=Ho, Dy, Tb, and Gd). Circle, square, and triangle denote T_{OO1}, T_{SO1}, and $T_{SO2}(=T_{OO2})$, respectively.

that the C-type spin/G-type orbital ordering remains down to 2 K.

Figures 3(a) and 3(b) show the phase diagram of the spin/orbital ordering for $Y_{1-x}Eu_xVO_3$ and that for RVO_3, respectively. The r_R dependence of T_{OO1} and T_{SO1} for $Y_{1-x}Eu_xVO_3$ is almost identical to those for RVO_3 with R=Y, Dy, Tb, and Gd; T_{OO1} and T_{SO1} monotonically increase with increasing x, or equivalently, r_R. This is not the case for T_{SO2} $(=T_{OO2})$. In the phase diagram of the spin/orbital ordering, the G-type spin/C-type orbital ordered phase subsists up to r_R =1.206 Å (x=0.52) for $Y_{1-x}Eu_xVO_3$ but is not discernible for $TbVO_3$ (r_R=1.203 Å). This indicates that the phase boundary between the G-type spin/C-type orbital ordered phase and the C-type spin/G-type orbital ordered phase cannot be uniquely determined by r_R, or equivalently by the magnitude of the $GdFeO_3$-type orthorhombic lattice distortion. One possibility would be the effect of the quenched disorder of the lattice sector for $Y_{1-x}Eu_xVO_3$, which might originate from the random substitution of Y with Eu. Yan *et al.*[17] have recently revealed that the quenched disorder of the lattice sector enhances T_{SO2} $(=T_{OO2})$ and stabilizes the G-type spin/C-type orbital ordered phase over the C-type spin/G-type orbital ordered one. They simultaneously observed the large reduction in T_{OO1} and T_{SO1}, as the quenched disorder of the lattice sector increases. This is, however, not the case for the present system; the r_R dependence of T_{OO1} and T_{SO1} for $Y_{1-x}Eu_xVO_3$ is almost identical to those for RVO_3 (R=Dy, Tb, and Gd) as previously mentioned. Therefore, the quenched disorder of the lattice sector cannot be the primary cause for the robustness of the G-type spin/C-type orbital ordered phase for $Y_{1-x}Eu_xVO_3$.

Another possible and more plausible factor is the magnetic exchange interaction between the V 3d spin and the Tb 4f moment for $TbVO_3$ in the form of $\Sigma_{ij}J_{ij}S_i^V \cdot S_j^R$. Here, S_i^V and S_j^R are the V 3d spin and R 4f moment, respectively. In the G-type spin/C-type orbital ordered phase with the *Pbnm* lattice symmetry, the easy axis of the V 3d spin is almost along the c axis, i.e., the G_c mode. Reehuis *et al.*[13] have reported that the ordering of the V 3d spin is in the $C_aC_bG_c$ mode in the C-type spin/G-type orbital ordered phase, and the ordering of the Tb 4f moment with the C_aF_b mode emerges at 11 K for $TbVO_3$. In addition, they pointed out that the ordering of the Tb 4f moment has been slightly induced even at 40 K, reflecting the spin ordering of the V sublattice. The energy gain due to the exchange interaction between the spin ordering of the V sublattice with the G_c mode and that of the Tb sublattice with the C_aF_b mode is zero while that between the spin ordering of the V sublattice and the ordering of the Tb 4f moment with C_a mode is finite. Thus, it is plausible that the exchange interaction between the V 3d spin and the Tb 4f moment stabilizes the C-type spin/G-type orbital ordering over the G-type spin/C-type orbital ordering in $TbVO_3$. The close interplay between the R 4f moment and the V 3d spin under the external magnetic field is discussed in the following sections with focusing on the case of R=Dy and Ho.

To see the spin/orbital ordered state more closely, we have investigated Raman scattering spectra for $Y_{1-x}Eu_xVO_3$. Figure 4(a) shows the Raman-scattering spectra for $Y_{1-x}Eu_xVO_3$ with various x at 4.3 K. For x=0, one can see two sharp peaks at 490 and 674 cm^{-1} as well as a broad band centered at 470 cm^{-1}. The peak at 490 cm^{-1} is assigned to the V-O-V bond bending vibration mode. The peak at 674 cm^{-1} is assigned to the V-O bond stretching vibration mode, which is strongly activated by the lattice distortion coupled to the C-type OO.[3,9] The broad band centered at 470 cm^{-1} is the two-magnon band characteristic of the G-type SO. A similar spectral feature is also observed for the doped system, x =0.2 and 0.4. By contrast, for x=0.55, 0.8, and 1.0, where the C-type spin/G-type orbital ordered phase emerges as the ground state, the peak at 674 cm^{-1} is smeared out and the V-O bond stretching vibration mode coupled to the G-type OO appears at 704 cm^{-1}.

To see the doping dependence of the spectral intensity of each mode more clearly, we fitted the two-magnon band and the V-O bond stretching mode with the Lorentz-type oscillator,

$$I(\omega) = \frac{S\omega_0^2\gamma\omega}{(\omega^2-\omega_0^2)^2+\omega_0^2\gamma^2} + I_{bg}. \quad (1)$$

Here, S is the spectral intensity, ω_0 the mode frequency, and γ the damping rate, I_{bg} the constant representing the back ground, respectively. We show S of each mode as a function of x in the inset of Fig. 4. As x increases, S of the V-O bond stretching mode coupled to the C-type OO (G-type OO) steeply decreases (increases) around x=0.5, corresponding to the phase transition from the G-type SO/C-type OO to the C-type SO/G-type OO. Similarly, S for the two-magnon band characteristic of the G-type SO decreases with x around x

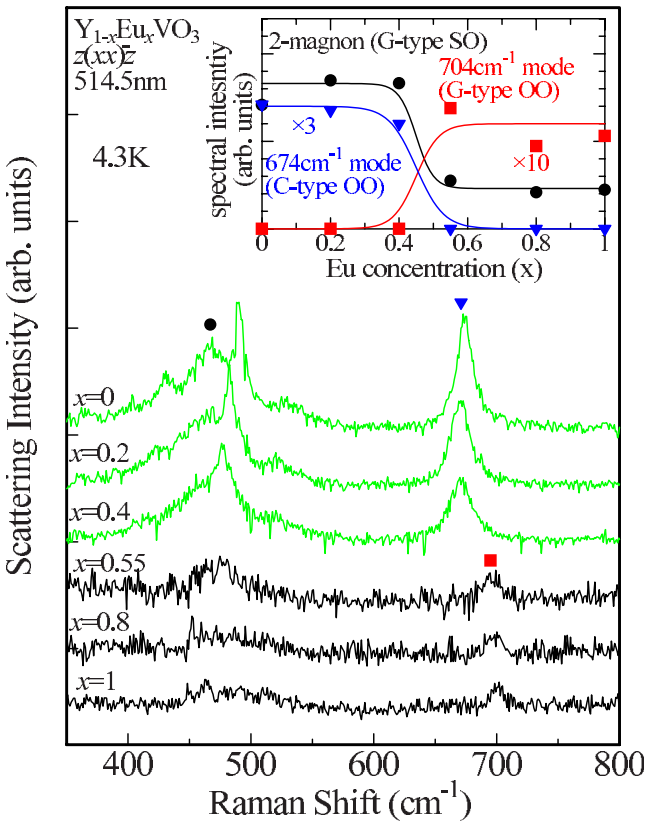

FIG. 4. (Color online) Raman-scattering spectra for the polarization configuration $z(xx)\bar{z}$ at 4.3 K. The spectra are vertically offset for clarity. Circle, triangle, and square indicate the two-magnon band characteristic of the G-type SO, the V-O stretching vibration coupled to the C-type OO and that coupled to the G-type OO, respectively. The inset shows the x dependence of the spectral intensity for the two-magnon band characteristic of the G-type SO (circle), the V-O stretching vibration coupled to the C-type OO (triangle) and the V-O stretching vibration coupled to the G-type OO (square).

=0.5 but remains finite even for $x>0.5$. One possible scenario to explain these results may be the dynamical fluctuation of the G-type spin/C-type orbital ordering in the nominally C-type spin/G-type orbital ordered phase. The subsistence of the two-magnon band is also seen in the hole doping induced C-type spin/G-type orbital ordered phase for $Y_{1-x}Ca_xVO_3$, and is interpreted in terms of the spin/orbital dynamical fluctuation.[18] As previously mentioned, the phase transition between the G-type spin/C-type orbital ordered state and the C-type spin /G-type orbital ordered one is, however, of first order. Thus, the dynamical fluctuation of the G-type SO/C-type OO in the nominally C-type spin/G-type orbital ordered phase at temperatures as low as 4.3 K would be unlikely. Another possible scenario is the coexistence of the G-type spin/C-type orbital ordered region (patch) in the nominally C-type spin/G-type orbital ordered phase. Recently, Sage *et al.*[19] have performed an x-ray diffraction measurement for RVO_3 and proposed that the G-type spin/C-type orbital ordered region subsists in the C-type spin/G-type orbital ordered phase at low temperatures. They suggest that the volume fraction of the G-type spin/C-type orbital ordered region in the nominally C-type spin/G-type orbital ordered state amounts to as large as 60% for $TbVO_3$ and $GdVO_3$, which is even not on the verge of the phase boundary in the spin/orbital phase diagram as shown in Fig. 3. In the phase coexistence model, the intensity of the two-magnon band characteristic of the G-type SO may be a good measure of the volume fraction of the G-type spin/C-type orbital ordered region. Following this simplified consideration, the volume fraction of the G-type spin/C-type orbital ordered region for $x=0.55$, which is located on the verge of the phase boundary, is approximately 30%. This value is much smaller than the reported one by Sage *et al.* This discrepancy may originate from the difference in the crystalline quality of the sample; we have investigated the single crystal in this study while Sage *et al.* have done the experiments using the polycrystalline powder. The crystalline inhomogeneity such as the mechanical strain at the grain boundary in the ceramics may enhance the phase coexistence of the competing spin/orbital ordered states. The effect of the $R\,4f$ moment on such a phase coexistence will be discussed in the next section.

B. Magnetic field induced phase transition of the spin/orbital ordering in $DyVO_3$

In this section, we present the results for the magnetic field induced phase transition of the spin/orbital ordering in $DyVO_3$ investigated by measurements of magnetization, dielectric constant, Raman-scattering spectra and x-ray diffraction.

First, we discuss the data measured in zero magnetic field. Figures 5(a) and 5(b) show the x-ray diffraction profiles around the (401) Bragg reflection at various temperatures for $DyVO_3$. The (401) Bragg reflection is forbidden in the orthorhombic crystal structure with the *Pbnm* symmetry at room temperature but is allowed in the G-type orbital ordered phase with the $P2_1/b$ monoclinic crystal symmetry as observed in YVO_3.[12] As temperature decreases from 300 K, a peak structure appears below 190 K ($=T_{OO1}$), corresponding to the onset of the G-type OO. As shown in Fig. 5(c), the magnetization curve shows a steep increase at T_{SO1} (=113 K) due to the magnetic transition to the C-type SO. With further decreasing temperature, both the (401) Bragg reflection and magnetization undergo steep changes at 64 K ($=T_{SO2}=T_{OO2}$); an abrupt decrease in the (401) Bragg reflection intensity is observed concomitantly with the jump of the magnetization curve in accord with the phase transition from the C-type SO/G-type OO to the G-type SO/C-type OO. The temperature dependence of the dielectric constant also exhibits a jump at $T_{SO2}(=T_{OO2})$ as shown in Fig. 5(d). This suggests that the dielectric constant can also be a good probe to detect the phase transition of the spin/orbital ordering because of its sensitivity to the structural or electronic phase transition. The magnetization and dielectric constant exhibit a clear thermal hysteresis (not shown in the figure), indicating that this phase transition is of first order as in the case of YVO_3. The reentrant transition of the spin/orbital ordering phase occurs at 22 K ($=T^*_{OO2}=T^*_{SO2}$); the G-type SO/C-type OO changes again to the C-type SO/G-type OO. At T^*_{SO2} ($=T^*_{OO2}$), the dielectric and magnetization properties exhibit a

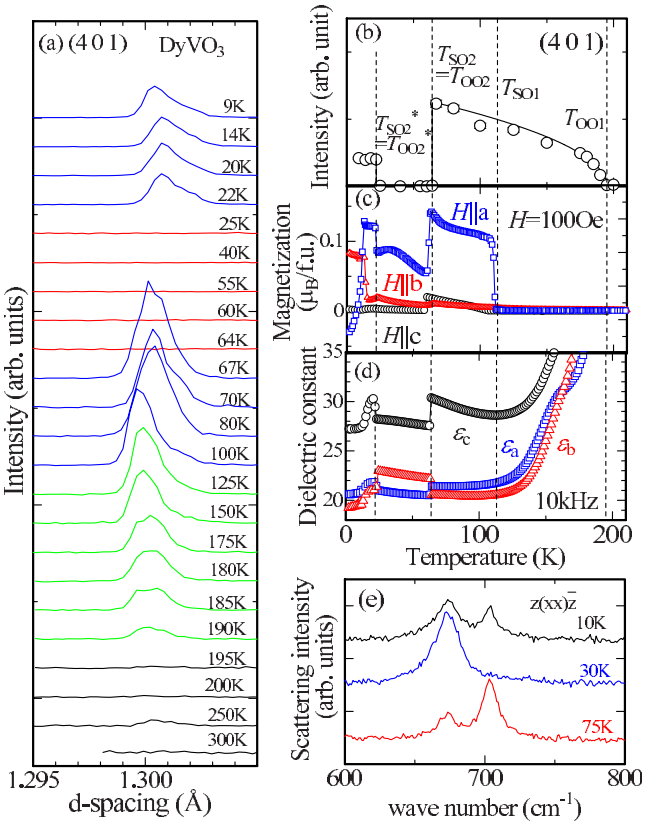

FIG. 5. (Color online) (a) (401) Bragg reflection at various temperatures. (b) The intensity of the (401) Bragg reflection plotted as a function of temperature. (c) Temperature dependence of the magnetization for $H\|a$ (blue squares), $H\|b$ (red triangles) and $H\|c$ (black circles), respectively. (d) Temperature dependence of the dielectric constant for $E\|a$ (blue squares), $E\|b$ (red triangles) and $E\|c$ (black circles), respectively. (e) Raman-scattering spectra with the polarization configuration $z(xx)\bar{z}$ at 10 K(black), 30 K(blue), and 75 K(red). Spectra are vertically offset for clarity.

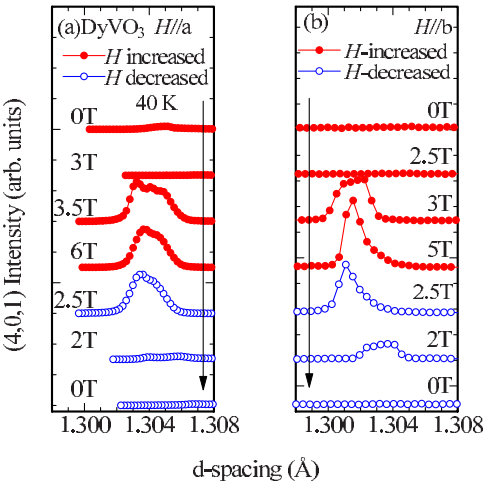

FIG. 6. (Color online) Profiles of the (401) Bragg reflection in various magnetic fields for (a) $H\|a$ and (b) $H\|b$. Closed (open) circles represent the profiles measured with increasing (decreasing) the magnetic field. Vertical arrow indicates the way of the scans.

steep change with a clear thermal hysteresis, which is consistent with the temperature dependence of the (401) Bragg reflection intensity (not shown in the figure).[20]

It should be noted that the intensity of the (401) Bragg reflection at 9 K is much smaller than that at 67 K. This is perhaps because the G-type spin/C-type orbital ordered region subsists even below T^*_{SO2} ($=T^*_{OO2}$) in the nominally C-type spin/G-type orbital ordered phase. In the phase coexistence model, the intensity of the (401) Bragg reflection would be proportional to the volume fraction of the C-type spin/G-type orbital ordered region. Although we do not know the intensity of the (401) Bragg reflection in the C-type spin/G-type orbital ordered state at 9 K without the phase coexistence, the ratio of the intensity of the (401) Bragg reflection at 9 K to that at 67 K is about 1/3. Thus, it is expected that the converted volume fraction of the C-type spin/G-type orbital ordered matrix is at most 1/3.

The phase coexistence state can be also probed by the Raman scattering spectra. In Fig. 5(e), we show the Raman-scattering spectra with the polarization configuration $z(xx)\bar{z}$ at 10, 30, and 75 K. At 75 K, two peaks are observed around 670 and 703 cm^{-1}, which are assigned to the V-O stretching mode activated by the lattice distortion coupled to the G-type OO. The intensity of 703 cm^{-1} mode is larger than that of 670 cm^{-1} mode. At 60 K in the G-type spin/C-type orbital ordered phase, the 703 cm^{-1} mode disappears while the 670 cm^{-1} mode remains discernible. These features are similar to the case for the $Y_{1-x}Eu_xVO_3$ with $x=0-0.52$ as remarked in the previous section. At 10 K, i.e., below T^*_{SO2} ($=T^*_{OO2}$), the 703 cm^{-1} mode again emerges while its spectral intensity seems to be smaller than that at 75 K. It should be noted that the spectral intensity of 670 cm^{-1} mode is even larger than that of 703 cm^{-1} mode, suggesting the heavy phase mixture of the G-type spin/C-type orbital ordered region with the C-type spin/G-type orbital ordered one. By comparing the intensity of 703 cm^{-1} at 10 K to that at 75 K, the volume fraction of the converted C-type spin/G-type orbital ordered region amounts to around 40%, which is almost consistent with the estimated value by the (401) Bragg reflection. Such a phase coexistent nature probably originates from the keen competition between the G-type spin/C-type orbital ordered state and the C-type spin/G-type orbital ordered one.

The phase switching between the G-type spin/C-type orbital ordered phase to the C-type spin/G-type orbital ordered one can be also achieved by applying the external field.[8,9] To clarify this issue, we have investigated the field dependence of the magnetization, dielectric property and (401) Bragg reflection. In Fig. 6(a), we show the (401) Bragg reflection as an indication of the G-type OO in various fields for $H\|a$ while fixing temperature at 40 K. At $H=0$ T, the (401) Bragg reflection is not observed, reflecting the *Pbnm* crystal symmetry in the G-type spin/C-type orbital ordered phase. As the magnetic field is increased, the (401) Bragg reflection appears above $H=3.5$ T but again disappears below $H=2$ T with decreasing the magnetic field. This evidences that the G-type OO with the $P2_1/b$ crystal symmetry emerges in higher magnetic fields. Here, the asymmetry in the peak shape may reflect the crystal mosaicness of samples, which often emerges after crossing the phase transitions by tem-

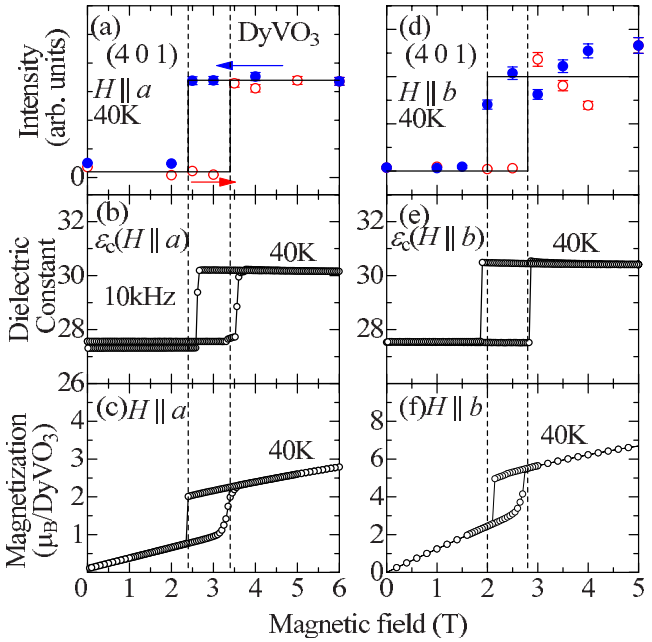

FIG. 7. (Color online) Magnetic field dependence of (a) the intensity of (401) Bragg reflection, (b) dielectric constant along the c axis measured at 10 kHz [ϵ_c(10 kHz)] and (c) magnetization for $H\|a$ at 40 K. Those for $H\|b$ are shown in (d), (e), and (f), respectively. Arrows indicate the direction of the field scan.

perature or magnetic field sweeping. Since the change in the peak shape may originate from the change in the sample quality, we do not discuss its temperature or field dependence here. Figures 7(a)–7(c) show the magnetic field dependence of the intensity of the (401) Bragg reflection, dielectric constant along the c-axis measured at 10 kHz [ϵ_c(10 kHz)] and magnetization at 40 K, respectively. The field dependence of the intensity of the (401) Bragg reflection shows a clear hysteresis; it shows a sudden jump at H=3.5 T (H=2.5 T) with increasing (decreasing) the magnetic field. Such a hysteretic jump is also observed in the field dependence of ϵ_c(10 kHz) and the magnetization as shown in Figs. 7(b) and 7(c). The jump of magnetization amounts to more than 1 μ_B and the magnetization at 6 T exceeds 2.5 μ_B. This evidences that the field induced phase transition from the G-type spin/C-type orbital ordering to the C-type spin/G-type orbital ordering accompanies the discontinuous increase in the magnetization of the Dy 4f moment since the magnetic moment of the V 3d spin is at most 2 μ_B. A similar behavior is observed in the case for $H\|b$ as shown in Fig. 6(b) and Figs. 7(d)–7(f).

To get insight into the temperature dependence of the spin/orbital ordered state at high magnetic field, the profiles of the (401) Bragg reflection at various temperatures in H =0 T, H=6 T for $H\|a$ and H=5 T for $H\|b$ are shown in Figs. 8(a)–8(c), respectively. The results at H=0 T again confirm the orbital reentrant phase transition. At H=6 T for $H\|a$, the peak of the (401) Bragg reflection is discernible down to 10 K, indicating that the crystal structure remains to be monoclinic $P2_1/b$, that is, the G-type OO. A similar behavior is observed in the case of $H\|b$.

The temperature dependence of the intensity of the (401) Bragg reflection, dielectric constant and magnetization at H

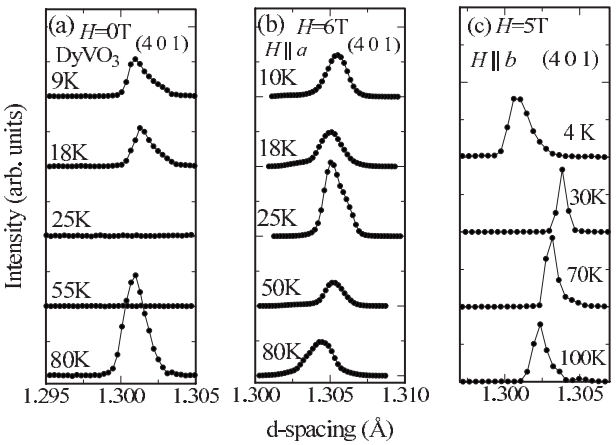

FIG. 8. Profiles of the (401) Bragg reflection at various temperatures in the magnetic field (a) 0 T, (b) 6 T for $H\|a$, and (c) 5 T for $H\|b$.

=0 T and H=6 T are displayed in Figs. 9(a)–9(c), respectively. As temperature decreases, the intensity of the (401) Bragg reflection at H=6 T monotonically increases down to the lowest temperature. The data are scattered especially at low temperatures perhaps because of the sample mosaicness as previously remarked. The dielectric constant at H=6 T does not show any jumps as observed at T_{SO2} ($=T_{OO2}$) and T^*_{SO2} ($=T^*_{OO2}$) for the case of H=0 T.[20] The magnetization also monotonically increases without any jump with decreasing temperature below T_{SO1}, and exceeds 4 μ_B at 2 K. These results suggest that the C-type spin/G-type orbital ordering subsists down to the lowest temperature below T_{SO1} at 6 T. A similar behavior is observed in the case of $H\|b$ (5 T) as shown in Figs. 9(d)–9(f).

It should be noted that the intensity of the (401) Bragg reflection is almost saturated below 60 K. This suggests that

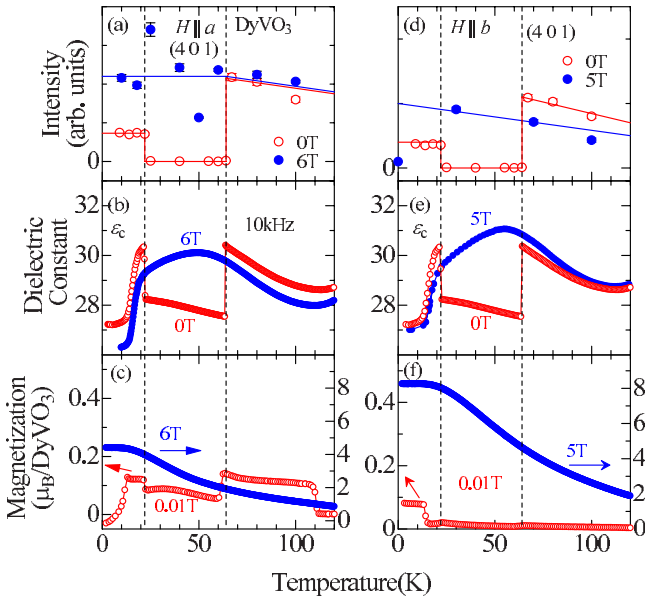

FIG. 9. (Color online) Temperature dependence of (a) the intensity of the (401) Bragg reflection, (b) dielectric constant, and (c) magnetization for $H\|a$, respectively. Those for $H\|b$ are shown in (d), (e), and (f), respectively.

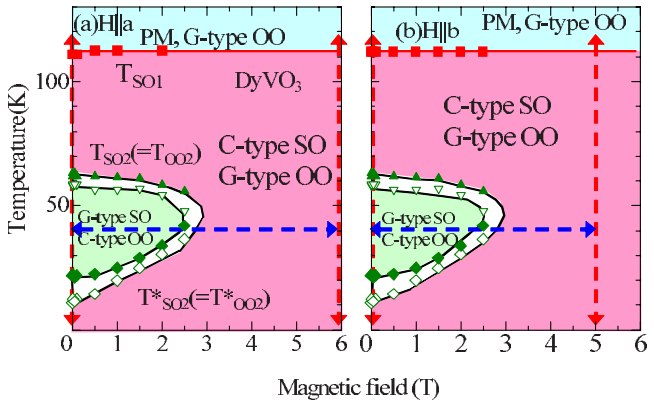

FIG. 10. (Color online) Phase diagram of the spin/orbital ordering in $DyVO_3$ for (a) $H\|a$ and (b) $H\|b$, respectively, as reproduced from Refs. 8 and 9. Closed squares, triangles, and diamonds represent T_{SO1}, T_{SO2} $(=T_{OO2})$, and T^*_{SO2} $(=T^*_{OO2})$, respectively, which are measured in the warming process. Open triangles and diamonds are T_{SO2} and T^*_{SO2}, respectively, which are measured in the cooling process. Hatched region corresponds to the hysteresis region. Vertical (horizontal) dashed arrows indicate the way of the temperature (magnetic field) scanning of the (401) Bragg reflection measurement for the present study.

the G-type spin/C-type orbital ordered region as observed below T^*_{SO2} $(=T^*_{OO2})$ at $H=0$ T is no longer present at $H=6$ T. In other words, the magnetic field appears to completely wipe out the residual G-type spin/C-type orbital ordered region. This is because the external magnetic field enhances the ordering of the Dy $4f$ moment, which favors the C-type spin/G-type orbital ordering, and hence more destabilizes the G-type spin/C-type orbital ordered region. It is thus evident that the R $4f$ moment plays an important role to control the phase coexistence of the competing spin/orbital ordered states of the V $3d$ sublattice.

To summarize the spin/orbital ordered state in the magnetic field, we showed the spin/orbital phase diagram on the temperature versus the magnetic field plane for $H\|a$ and $H\|b$ in Figs. 10(a) and 10(b), respectively. It is evident that the G-type spin/C-type orbital ordered phase is replaced by the C-type spin/G-type orbital ordered one in higher magnetic fields than 3 T for both $H\|a$ and $H\|b$; T^*_{SO2} $(=T^*_{OO2})$ monotonically increases by applying the external magnetic field and exceeds 40 K around $H=2.5$ T while T_{SO2} slightly decreases and appears to coincide with T^*_{SO2} around $H=3$ T.

The observed field induced phase transition that accompanies the concomitant magnetization change in the Dy $4f$ moment may be explained in terms of the exchange interaction between the Dy $4f$ moment and the V $3d$ spin. Reehuis *et al.*[21] have revealed by a neutron-diffraction experiment that the Dy $4f$ moment orders in the F_aC_b mode below 23 K, and in the C_aF_b mode below 13 K. Such thermally induced sequential magnetic phase transitions suggest that these two types of Dy $4f$ moment ordering are almost degenerate in free energy and hence Dy $4f$ moment can be easily polarized in the F_aC_b (C_aF_b) mode in the moderate magnetic fields for $H\|a$ $(H\|b)$. The mechanism of the field induced phase transition for $H\|b$ is simple; the ordering of the V $3d$ spin is almost in the G_c mode for the G-type spin/C-type orbital ordered phase, where the exchange interaction between the Dy $4f$ moment and the V $3d$ spin is zero as discussed in the previous section. From the viewpoint of the group theory, the magnetic component of the V $3d$ spin in the C_aF_b mode is forbidden in the G-type spin/C-type orbital ordered phase with the G_c mode and the *Pbnm* crystal symmetry. Thus, the energy gain of the exchange interaction between the Dy $4f$ moment and the V $3d$ spin may be negligibly small in the moderate magnetic field. By contrast, the ordering of the V $3d$ spin is in the $C_aC_bG_c$ mode for the C-type spin/G-type orbital ordered phase.[13] In this case, the energy gain due to the exchange interaction between the Dy $4f$ moment with the C_aF_b mode and the V $3d$ spin is finite. Thus, it is reasonable that the field induced ordering of the Dy $4f$ moment with the C_aF_b mode favors the C-type spin/G-type orbital ordering for $H\|b$.

On the contrary, the mechanism of the field induced phase transition to the C-type spin/G-type orbital ordered phase for $H\|a$ is not straightforward. The $F_aC_bG_c$ mode of the V $3d$ spin ordering is allowed in the G-type spin/C-type spin ordered state with the *Pbnm* crystal symmetry for $H\|a$. Thus, the energy gain due to the exchange interaction between the Dy $4f$ moment and V $3d$ spin is finite in the F_aC_b mode. On the one hand, it is also finite owing to the presence of the C_b component in the C-type spin/G-type orbital ordered phase. In this case, the subtle balance of the energy gain of the exchange interaction between the Dy $4f$ moment and V $3d$ spin might determine which spin/orbital ordered phase is favored in the magnetic field. The quantitative explanation of the spin/orbital phase in the magnetic field, which requires the accurate information on the crystal and magnetic structure, will be left for the future study.

C. Spin/orbital ordering for $HoVO_3$ in the magnetic field

In this section, to get a further insight into the mechanism of the coupling between the R $4f$ moment and the spin/orbital ordering of the V $3d$ electron, we focus on the phase diagram of the spin/orbital ordering in the external magnetic field for $HoVO_3$ as investigated by the magnetization and the dielectric constant measurements. The r_R of Ho is smaller than that of the Dy and hence the $GdFeO_3$-type orthorhombic lattice distortion is larger in $HoVO_3$ than in $DyVO_3$ while the Ising-type Ho $4f$ moment $(\sim 10.58\ \mu_B)$ is comparable with the Dy one $(\sim 10.63\ \mu_B)$. The critical competition of the spin/orbital ordering as affected by the coupling between the Ho $4f$ moment and the spin/orbital sector of the V $3d$ electron is also observed in $HoVO_3$ as argued in the following.

We show the temperature dependence of the magnetization for $HoVO_3$ in Fig. 11(a). In the cooling process, the magnetization curve shows an increase at 111 K (T_{SO1}) in accord with the onset of the C-type SO for the V $3d$ sublattice. At lower temperatures, two jumps are discernible at 36 K $(=T'_{SO2})$ and 11 K $(=T_{SO2})$ as indicated by the triangle and the vertical dashed line, respectively. The latter corresponds to the magnetic transition from C-type (high-temperature phase) to G-type (low-temperature phase) while the origin of the former is not clear at the moment. Incidentally, T_{SO2} is

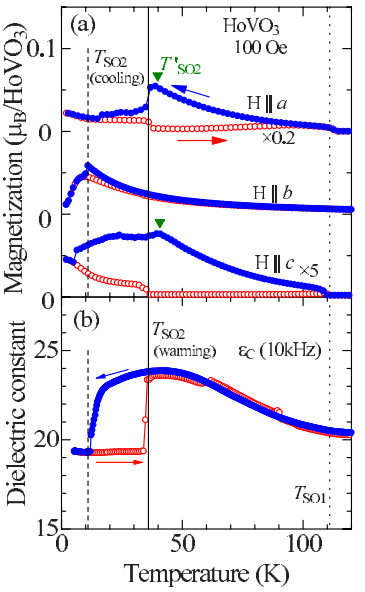

FIG. 11. (Color online) (a) Temperature dependence of the magnetization for $HoVO_3$ measured in the cooling (closed circles) and warming (open circles) process. The direction of the scan is indicated by arrows. The triangles indicate T'_{SO2}. The vertical dashed line indicates T_{SO2} measured in the cooling process. The vertical dotted and solid lines indicate T_{SO1} and T_{SO2} measured in the warming process, respectively. (b) Temperature dependence of the dielectric constant along the c axis measured at 10 kHz in the cooling (closed circles) and warming (open circles) process.

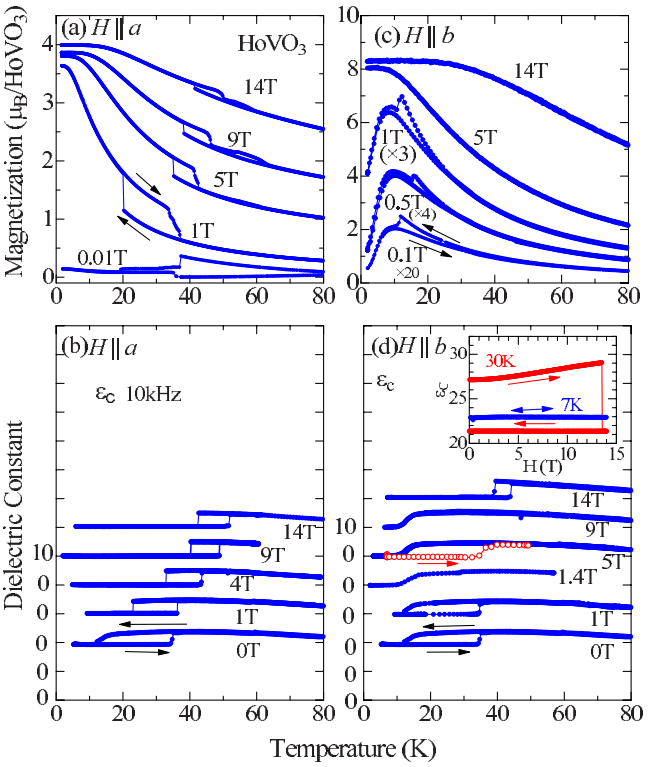

FIG. 12. (Color online) Temperature dependence of the (a) magnetization and (b) dielectric constant along the c axis measured at 10kHz [ϵ_c(10 kHz)] for $H \| a$. Those for $H \| b$ are shown in (c) and (d), respectively. The open circles in (d) indicate ϵ_c(10 kHz), which are measured in the warming process for $H=5$ T after cooling down to 2 K at zero magnetic field (see also text). The inset to (d) is the magnetic field dependence of ϵ_c(10 kHz) at 7 K (blue) and 30 K (red). Arrows indicate the direction of the magnetic field sweeping.

scattered in the range between 5 and 16 K and strongly depends on the sample quality. A small amount of impurities or the internal lattice strain in samples appear to critically affect this magnetic phase transition. In the warming process from the lowest temperature (2 K), the magnetic transition from G-type to C-type is discernible at 37 K in the magnetization curve for $H \| a$ and $H \| c$ as indicated by the vertical solid line. Figure 11(b) shows the temperature dependence of the dielectric constant along the c axis measured at 10 kHz [ϵ_c(10 kHz)]. The ϵ_c(10 kHz) curve shows a jump at T_{SO2} ($=T_{OO2}$) in accord with the magnetization curve, indicating the phase transition between the C-type SO/G-type OO (high-temperature phase) and the G-type SO/C-type OO (low-temperature phase).

Figures 12(a)–12(d) show the temperature variation in magnetization and ϵ_c(10 kHz) in various magnetic fields for $H \| a$ and $H \| b$. First, we present the results for $H \| a$ [Figs. 12(a) and 12(b)]. The magnetization and ϵ_c(10 kHz) for $H \| a$ indicate the phase transition from the G-type SO/C-type OO (low-temperature phase) to the C-type SO/G-type OO (high-temperature phase) at T_{SO2} ($=T_{OO2}$). Reehuis *et al.*[21] have recently shown by a neutron-diffraction experiment that the G-type SO/C-type OO accompanies the ordering of the Ho $4f$ moment. This is consistent with the steplike increase in magnetization at T_{SO2} ($=T_{OO2}$). With the increase in magnetic field, the magnetization monotonically increases in a wide temperature range below 80 K and T_{SO2} ($=T_{OO2}$) is also enhanced. For example, at $H=14$ T, the magnetization exceeds 2.5 μ_B even at 80 K and T_{SO2} ($=T_{OO2}$) is over 40 K. This suggests that the Ho $4f$ moment is significantly polarized even at high temperatures far above T_{SO2} and seriously influences on the spin/orbital ordering of the V sublattice in $HoVO_3$ as in the case of $DyVO_3$. Such a large enhancement of T_{SO2} ($=T_{OO2}$) by a magnetic field cannot be seen in YVO_3 with a nearly equal orthorhombic lattice distortion (see Fig. 1).

We now turn on the magnetization and dielectric properties for $H \| b$ as shown in Figs. 12(c) and 12(d). As temperature is lowered, a small cusp (jump) is observed around 12 K in the magnetization (dielectric constant) curve in a weak magnetic field below 1 T, which perhaps corresponds to the onset of the G-type SO/C-type OO. The thermal hysteresis is observed in the ϵ_c(10 kHz) curve but less obvious in the magnetization curve. The clear jump and thermal hysteresis are not discernible in the magnetization nor the ϵ_c(10 kHz) curve for a magnetic field region of 1.4 T$\leq H \leq$9 T, suggesting the absence of the spin/orbital phase switching down to 2 K. At $H=14$ T, however, the spin/orbital phase switching is again observed in the ϵ_c(10 kHz) curve with a clear jump and hysteresis.

To examine the occurrence of the spin/orbital phase switching for 1.4 T$\leq H \leq$9 T, first, we measured ϵ_c(10 kHz) at 7 and 30 K with sweeping the magnetic field as shown in the inset to the Fig. 12(d). At 30 K, where the

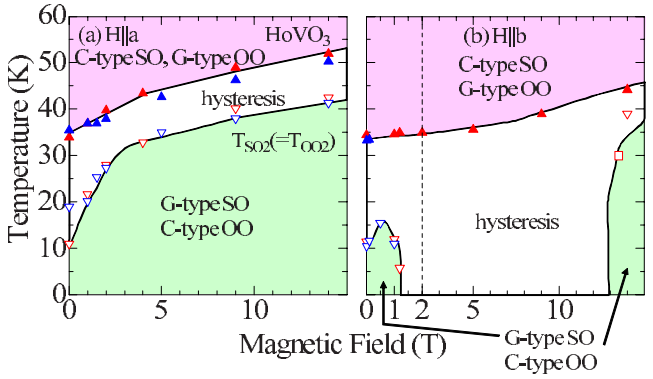

FIG. 13. (Color online) Phase diagram of the spin/orbital ordering in the magnetic fields for (a) $H\|a$ and (b) $H\|b$, respectively. Closed and open triangles indicate the T_{SO2} measured in the warming and cooling process, respectively. The hatched region denotes the hysteresis region. For (b), the scale of the magnetic field (horizontal axis) is magnified below $H=2$ T (dashed line).

C-type spin/G-type orbital ordering is realized in zero magnetic field after cooling from room temperature, the ϵ_c(10 kHz) curve shows a sudden drop around 13 T in the process of increasing magnetic field, signaling the phase switching of the spin/orbital ordering. By contrast, when the magnetic field is decreased from 14 T, no anomaly is discernible. This is not the case at 7 K, where the G-type spin/C-type orbital ordering is realized in zero magnetic field; the ϵ_c(10 kHz) curve does not show any anomalies up to 14 T, implying the absence of the field induced phase switching. Next, we measured the temperature dependence of ϵ_c(10 kHz) in the warming process at the fixed magnetic field after the zero-field cooling; we cooled the sample down to 7 K in zero magnetic field, applied the magnetic field up to 5 T, and then measured the ϵ_c(10 kHz) curve in the warming process while keeping the magnetic field at 5 T. As shown in Fig. 12(d) (open circles), the ϵ_c(10 kHz) curve measured in this process exhibits a jump at 35 K perhaps corresponding to the spin/orbital phase switching from the G-type SO/C-type OO (low-temperature phase) to the C-type SO/G-type OO (high-temperature phase).

Based on these results, we derive the spin/orbital phase diagram in the temperature versus magnetic field plane for $H\|a$ and $H\|b$ in Figs. 13(a) and 13(b), respectively. For $H\|a$, it is clear that T_{SO2} $(=T_{OO2})$ monotonically increases with the increase in magnetic fields, indicating that the G-type spin/C-type orbital ordered phase is dominant over the C-type spin/G-type orbital ordered phase at high magnetic fields. A similar situation is observed for $H\|b$, although the hysteresis region prevails over a wide range on the temperature versus the magnetic field plane. These results contrast with the case of $DyVO_3$, in which the C-type spin/G-type orbital ordered phase is favored at high magnetic fields. In zero magnetic field, it is recently known that the Ho $4f$ moment orders in the $F_aC_bG_c$ mode concomitantly with the onset of the G-type SO/C-type OO of the V $3d$ sublattice.[21] For $H\|a$, the spin ordering of the V $3d$ sublattice is allowed in the $F_aC_bG_c$ mode in the G-type spin/C-type orbital ordered phase with *Pbnm* crystal symmetry. In this case, the energy gain due to the exchange interaction between the Ho $4f$ moment and the V $3d$ spin is finite. Thus, if the energy gain due to the exchange interaction between the Ho $4f$ moment and the V $3d$ spin is larger in the G-type spin/C-type orbital ordered phase than in the C-type spin/G-type orbital ordered one, the former phase should be favored in high magnetic fields as observed.

For $H\|b$, the ordering of the Ho $4f$ moment is allowed in the C_aF_b mode with keeping the *Pbnm* crystal symmetry. In terms of the exchange interaction between the Ho $4f$ moment and the V $3d$ spin in the form of $\Sigma_{ij}J_{ij}S_i^V\cdot S_j^R$, the field induced ordering of the Ho $4f$ moment would rather favor the C-type SO of the V $3d$ sublattice as observed in $DyVO_3$ but contrary to what is observed for $HoVO_3$. Then, one may think that the antisymmetric magnetic exchange interaction between the V $3d$ spin and R $4f$ moment in the form of the $\Sigma_{ij}\vec{D}_{ij}\cdot(S_i^V\times S_j^R)$ plays some roles in this phase transition. According to Ref. 22, however, this mechanism also does not allow the coupling between the V $3d$ spin ordering in the G_c mode and the Ho $4f$ moment ordering in the C_aF_b mode for the *Pbnm* lattice symmetry.

One possible scenario is the interaction between the Ho $4f$ moment and the lattice distortion coupled to the orbital ordering in the V sublattice. The R $4f$ moment generally interacts with the lattice distortion via the change in the crystal field at R site to produce the change in the single ion anisotropy. The energy scale of such an effect on the $4f$ moment is, however, negligible in a conventional structural phase transition. In the present case, the typical magnitude of the displacement of R ion during the phase transition between the G-type spin/C-type orbital ordered state and C-type spin/G-type orbital ordered one is 6×10^{-3} Å, which is the order of 10^{-3} of the R V bond length. At the moment, it is not clear whether such a tiny ion displacement can produce the enough change in the single ion anisotropy of R ion to give rise to the field-induced phase transition. Another possibility is that the spin/orbital ordering is no longer G-type/C-type in the finite magnetic field; the V $3d$ spin ordering in the $C_aF_bA_c$ mode, which is also allowed spin configuration in the *Pbnm* lattice symmetry and can be coupled to the Ho $4f$ moment ordering in the C_aF_b mode, is mixed with that in the G_c mode. Similar field induced spin reorientation transitions are also observed in the rare-earth orthoferrites.[23] Since the fingerprint of the field-induced phase switching could not be detected by the magnetization or the dielectric constant as presented above, it is the issue of the future to clarify the spin/orbital ordering in magnetic fields by means of the diffraction experiments.

IV. CONCLUSION

In conclusion, we have investigated the critical competition of the spin/orbital ordered phases in the rare-earth orthovanadates RVO_3 (R is rare-earth ion) by measurements of magnetization, dielectric constant, specific heat, Raman-scattering spectra, and synchrotron x-ray diffraction, focusing on the interplay between the V $3d$ spin and the R $4f$ moment.

First, we have revealed the spin/orbital phase diagram for $Y_{1-x}Eu_xVO_3$, where the $GdFeO_3$-type orthorhombic crystal

distortion can be systematically controlled by changing x like the variation in other R ions but the $4f$ moment of R site is absent. The thermally induced phase transition between the C-type spin/G-type orbital ordered state and the G-type spin/C-type orbital ordered one is identified for $x=0-0.52$. From the comparison of the phase diagram of the spin/orbital ordering for $Y_{1-x}Eu_xVO_3$ with that for $TbVO_3$, it is evident that the C-type spin/G-type orbital ordering is stabilized by the presence of the Tb $4f$ moment. The energy gain due to the coupling between the spin ordering of the V sublattice in the C_a,C_b,G_c mode and the Tb $4f$ moment ordering in the F_a,C_b mode is finite by assuming the Heisenberg-type spin exchange interaction in the form of $\Sigma_{ij}J_{ij}(\vec{S_i^V}\cdot\vec{S_j^R})$.

It is demonstrated that the spin/orbital phase switching is induced by the magnetic field in $DyVO_3$ accompanying the polarization of the R $4f$ moment. We identified the field-induced phase transition by observation of sudden changes of the magnetization and dielectric properties as well as the (401) Bragg reflection allowed by the lattice distortion coupled to the G-type OO. The G-type spin/C-type orbital ordered state is switched to the C-type spin/G-type orbital ordered one concomitantly with the discontinuous increase in the polarization of the Dy $4f$ moment in a moderate magnetic field around 3 T. In $HoVO_3$, a similar field-induced phase transition is identified by measurements of the magnetization and dielectric properties; the G-type spin/C-type orbital ordered state appears to be rather favored than the C-type spin/G-type orbital ordered one in magnetic fields.

These field induced phase transitions can be consistently explained by the Heisenberg type magnetic exchange interaction between the V $3d$ spin and R $4f$ moment except the case of $H\|b$ for the $HoVO_3$. For the latter, the energy gain due to the coupling between the V $3d$ spin ordering in the G_c mode and Ho $4f$ moment ordering in the C_aF_b mode is zero even by assuming the antisymmetric magnetic exchange interaction in the form of $\Sigma_{ij}\vec{D_{ij}}\cdot(\vec{S_i^V}\times\vec{S_j^R})$. One possible origin of this discrepancy is that the coupling between the V $3d$ electron and R $4f$ moment depends not only on the magnetic exchange interaction but also on the interaction between the R $4f$ moment and the lattice distortion tied with the orbital ordering in the V $3d$ sublattice, which may manifest itself as the change in the single ion anisotropy of R $4f$ moment. The typical magnitude of the displacement of R ion across the phase transition between the G-type spin/C-type orbital ordered state and C-type spin/G-type orbital ordered one is 6×10^{-3} Å, which is the order of 10^{-3} of the R V bond length. At the moment, it is not clear whether such a tiny ion displacement produces the enough change in the single ion anisotropy of the R $4f$ moment to give rise to the observed phase switching. Another possibility is that the spin/orbital ordering is no longer pristine G-type/C-type in magnetic fields; other spin configurations such as the $C_aF_bA_c$ mode is mixed with the G_c mode.

ACKNOWLEDGMENTS

The authors wish to thank B. Keimer, M. Reehuis, Y. Tokunaga, and H. Sakai for fruitful discussions. This work was in part supported by Grants-In-Aid (Grants No. 16740192, No. 17340104, No. 15104006, and No. 20110003) from JSPS and MEXT, Japan.

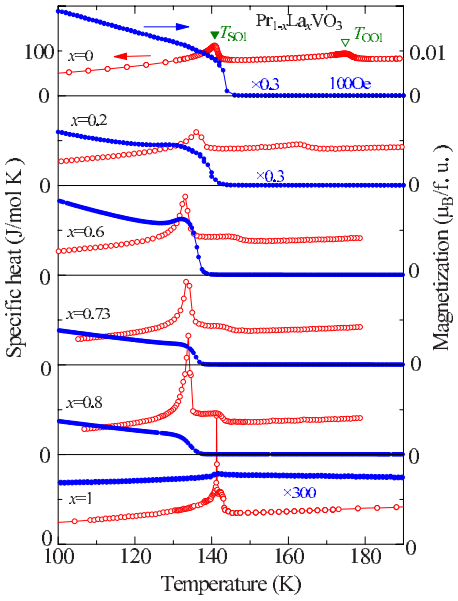

FIG. 14. (Color online) Temperature dependence of the specific heat (open circles) and magnetization (closed circles) for $Pr_{1-x}La_xVO_3$ with various x. Closed and open triangles indicate T_{SO1} and T_{OO1}, respectively.

APPENDIX: THE SPIN/ORBITAL PHASE DIAGRAM IN $Pr_{1-x}La_xVO_3$

To address the issue of the inversion of the G-type OO temperature (T_{OO1}) and the C-type SO one (T_{SO1}) in between R=Pr and La (Fig. 1), we have investigated the spin/orbital phase diagram for the mixed crystals of $Pr_{1-x}La_xVO_3$. Since the r_R of La is larger than that of Pr, the $GdFeO_3$-type orthorhombic lattice distortion is systematically reduced with increasing x. Figure 14 shows the temperature dependence of magnetization and specific heat for $Pr_{1-x}La_xVO_3$ with various x. For $x=0$ ($PrVO_3$), the onset of the G-type OO and the C-type SO are observed as a peak structure in the specific heat curve at $T_{OO1}=175$ K and $T_{SO1}=140$ K, respectively.

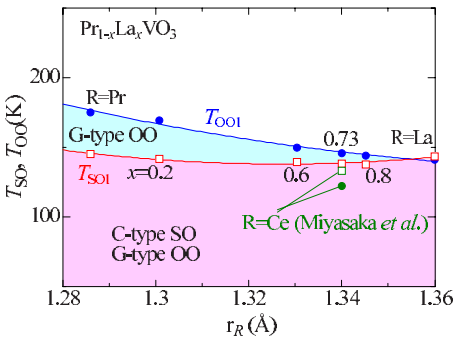

FIG. 15. (Color online) Phase diagram of the spin/orbital ordering for $Pr_{1-x}La_xVO_3$. Circles and squares indicate T_{OO1} and T_{SO1}, respectively (see text). The transition temperature of the spin/orbital ordering for $CeVO_3$ reported in Ref. 3 is also shown.

T_{SO1} can be also identified as an increase in the magnetization curve. We show the spin/orbital phase diagram for $Pr_{1-x}La_xVO_3$ in Fig. 15 by plotting T_{OO1} and T_{SO1} as a function of r_R, or equivalently, x. As x increases, the temperature interval between T_{OO1} and T_{SO1} is gradually reduced and finally T_{OO1} becomes lower than T_{SO1} at $x=1$ ($LaVO_3$). This behavior contrasts with the previous report by Miyasaka *et al.*,[3] in which the discontinuous jump of T_{OO1} as a function of r_R is expected in between R=Pr and Ce. The peak at T_{SO1} in the specific-heat curve becomes sharp and a discontinuous jump is observed for $x=1$. This suggests the first-order nature of the C-type SO is enhanced as T_{OO1} approaches to T_{SO1}. It should be noted that T_{OO1} is still higher than T_{SO1} for $x=0.73$, in which r_R is almost identical to that of $CeVO_3$. Ren *et al.*[24] have recently identified the second order (first-order) phase transition of the G-type OO (C-type SO) at $T_{OO1}=154$ K ($T_{SO1}=134$ K) for $CeVO_3$. This is consistent with the present results. T_{OO1} and T_{SO1} appears to change continuously with decreasing the $GdFeO_3$-type lattice distortion, at least, close up to $LaVO_3$.

[1] M. Imada, A. Fujimori, and Y. Tokura, Rev. Mod. Phys. **70**, 1039 (1998).

[2] Y. Tokura, Rep. Prog. Phys. **69**, 797 (2006).

[3] S. Miyasaka, Y. Okimoto, M. Iwama, and Y. Tokura, Phys. Rev. B **68**, 100406(R) (2003).

[4] C. Ulrich, G. Khaliullin, J. Sirker, M. Reehuis, M. Ohl, S. Miyasaka, Y. Tokura, and B. Keimer, Phys. Rev. Lett. **91**, 257202 (2003).

[5] Y. Motome, H. Seo, Z. Fang, and N. Nagaosa, Phys. Rev. Lett. **90**, 146602 (2003).

[6] P. Horsch, A. M. Oles, L. F. Feiner, and G. Khaliullin, Phys. Rev. Lett. **100**, 167205 (2008).

[7] J. Fujioka, S. Miyasaka, and Y. Tokura, Phys. Rev. B **72**, 024460 (2005).

[8] J. S. Zhou, J. B. Goodenough, J. Q. Yan, and Y. Ren, Phys. Rev. Lett. **99**, 156401 (2007).

[9] S. Miyasaka, T. Yasue, J. Fujioka, Y. Yamasaki, Y. Okimoto, R. Kumai, T. Arima, and Y. Tokura, Phys. Rev. Lett. **99**, 217201 (2007).

[10] P. Bordet, C. Chaillout, M. Marezio, A. Santoro, S. W. Cheong, H. Takagi, C. S. Oglesby, and B. Batlogg, J. Solid State Chem. **106**, 253 (1993).

[11] H. Kawano, H. Yoshizawa, and Y. Ueda, J. Phys. Soc. Jpn. **63**, 2857 (1994).

[12] G. R. Blake, T. T. M. Palstra, Y. Ren, A. A. Nugroho, and A. A. Menovsky, Phys. Rev. B **65**, 174112 (2002).

[13] M. Reehuis, C. Ulrich, P. Pattison, B. Ouladdiaf, M. C. Rheinstadter, M. Ohl, L. P. Regnault, M. Miyasaka, Y. Tokura, and B. Keimer, Phys. Rev. B **73**, 094440 (2006).

[14] M. Noguchi, A. Nakazawa, S. Oka, T. Arima, Y. Wakabayashi, H. Nakao, and Y. Murakami, Phys. Rev. B **62**, R9271 (2000).

[15] Y. Ren, T. T. M. Palstra, D. I. Khomskii, E. Pellegrin, A. A. Nugroho, A. A. Menovsky, and G. A. Sawatzky, Nature (London) **396**, 441 (1998).

[16] J. Q. Yan, J. S. Zhou, and J. B. Goodenough, Phys. Rev. B **72**, 094412 (2005).

[17] J. Q. Yan, J. S. Zhou, J. B. Goodenough, Y. Ren, J. G. Cheng, S. Chang, J. Zarestky, O. Garlea, A. Llobet, H. D. Zhou, Y. Sui, W. H. Su, and R. J. McQueeney, Phys. Rev. Lett. **99**, 197201 (2007).

[18] J. Fujioka, S. Miyasaka, and Y. Tokura, Phys. Rev. B **77**, 144402 (2008).

[19] M. H. Sage, G. R. Blake, C. Marquina, and T. T. M. Palstra, Phys. Rev. B **76**, 195102 (2007).

[20] The steep drop in the dielectric constant curve below 20 K reflects its frequency dependency. Thus, this does not correspond to the phase transition at T^*_{OO2} but originates from the Debye-type dielectric dispersion.

[21] M. Reehuis, C. Ulrich, K. Prokes, S. Matas, J. Fujioka, S. Miyasaka, Y. Tokura, and B. Keimer (unpublished).

[22] T. Yamaguchi, J. Phys. Chem. Solids **35**, 479 (1974).

[23] Y. Tokunaga, S. Iguchi, T. Arima, and Y. Tokura, Phys. Rev. Lett. **101**, 097205 (2008).

[24] Y. Ren, A. A. Nugroho, A. A. Menovsky, J. Strempfer, U. Rutt, F. Iga, T. Takabatake, and C. W. Kimball, Phys. Rev. B **67**, 014107 (2003).